Characterization of a chemical amplifier for peroxy radical measurements in the atmosphere

Marius Duncianu, Ahmad Lahib, Alexandre Tomas, Philip Stevens, Sébastien Dusanter

Characterization of a chemical amplifier for peroxy radical measurements in the atmosphere

Marius Duncianu[a], Ahmad Lahib[a,b], Alexandre Tomas[a], Philip S. Stevens[b,c], and Sébastien Dusanter[a,*]

[a]IMT Lille Douai, Université de Lille, SAGE – Département Sciences de l'Atmosphère et Génie de l'Environnement, 59000 Lille, France

[b]School of Public and Environmental Affairs, Indiana University, Bloomington, IN 47405, USA

[c]Department of Chemistry, Indiana University, Bloomington, IN 47405, USA

*Corresponding author: email: sebastien.dusanter@imt-lille-douai.fr ; Phone: +33327712623 ; IMT Lille Douai, SAGE department, 941 rue Charles Bourseul, 59508 Douai, France

Abstract

Peroxy radicals (HO_2 and RO_2) are key species in atmospheric chemistry. They are produced during the oxidation of volatile organic compounds (VOCs) and are involved in the formation of photochemical pollutants such as ozone (O_3) and secondary organic aerosols (SOA). However, ambient measurements of these reactive species are still challenging and only a few techniques can achieve both a good selectivity and a detection limit that is low enough for ambient measurements. In this publication we present the characterization of a Chemical Amplifier (CA) using two different approaches for ambient measurements of peroxy radicals, including the PEroxy Radical Chemical Amplifier (PERCA) and the Ethane based CHemical AMPlification (ECHAMP). At 50% Relative Humidity (RH), the experimental CL for PERCA was found to be higher by approximately a factor of 3.7 compared to ECHAMP. The RH-dependence of the CL was also found to be larger for PERCA by a factor of 1.12. Box modeling of the chemistry taking place in the instrument highlighted that the formation of HNO_3 from the HO_2+NO reaction has a strong impact on the CL for both approaches. In addition, experiments conducted to quantify the RO_2–to-HO_2 conversion efficiency for a large range of organic peroxy radicals confirmed that it mainly depends on the organic nitrate ($RONO_2$) formation yield, while the alkyl nitrite (RONO) yield is not limiting the CL in most cases. Ambient measurements using the PERCA approach are shown to illustrate the performances of this new instrument.

Keywords: Instrument development; peroxy radical chemical amplifier; PERCA; ECHAMP; atmosphere

1 Introduction

Due to their high reactivity, and therefore short lifetime, peroxy radicals (HO_2, and RO_2, R = $C_xH_yO_z$) are key species in atmospheric chemistry. These radicals are mainly produced when the OH radical reacts with CO, the abundant greenhouse gas methane and volatile organic compounds (VOCs). They are also formed through the photolysis of carbonyl compounds, reactions of alkenes with ozone, and some nighttime reactions involving the NO_3 radical and VOCs (Finlayson-Pitts and Pitts, 2000).

In the atmosphere, there is a rapid propagation chemistry between peroxy radicals, alkoxy radicals (RO) and the hydroxyl radical (OH), forming a group of species known as "ROx" (ROx ≡ HO_2 + RO_2 + RO + OH). Of particular interest, reactions of peroxy radicals with nitric oxide (NO) play a central role in tropospheric chemistry. Indeed, peroxy radicals propagate to OH, which sustains the oxidizing capacity of the atmosphere, and which converts NO into nitrogen dioxide (NO_2), whose photolysis leads to ozone formation. Organic peroxy radicals also play a key role as intermediates in the formation of secondary organic aerosols (SOA) (Kroll and Seinfeld, 2008). Both of these secondary pollutants, O_3 and SOA, are known to cause severe health effects. Together with OH, peroxy radicals therefore control the global oxidizing capacity of the Earth's atmosphere, and as a consequence, the concentration and distribution of greenhouse gases and secondary pollutants. Understanding the spatial and temporal variability of these radicals and being able to model this variability is key to evaluate future changes in the chemical composition of the atmosphere, with implications for both air quality and climate change.

Despite their important role in the atmosphere, the chemistry of peroxy radicals has yet to be fully understood under a wide range of atmospheric conditions, including remote locations (marine boundary layer) (Berresheim et al., 2002; Creasey et al., 2003), continental low-NO_x regions influenced by biogenic emissions (Archibald et al., 2011; Griffith et al., 2013; Wolfe et al., 2011), polluted urban areas (Dusanter et al., 2009; Volkamer et al., 2010), and polar regions (Mao et al., 2010; Read et al., 2008). Some of these studies have reported significant differences between measured and modeled concentrations of RO_x species likely due to an incomplete characterization of ambient trace gases and the use of incomplete chemical mechanisms in models. For instance, peroxy radical measurements can be significantly lower (Griffith et al., 2013) or higher (Wolfe et al., 2014) than model predictions in forested areas and significant missing OH sinks, likely leading to an underestimation of the OH-to-peroxy radical

propagation rate, have been reported for forested (Griffith et al., 2013; Heard and Pilling, 2003; Stone et al., 2012) and urbanized (Dusanter et al., 2009; Griffith et al., 2016; Volkamer et al., 2010) areas.

Measuring peroxy radicals is particularly difficult due to their reactive nature and their low ambient concentrations, which requires highly sensitive techniques with inlets designed to avoid the loss of the targeted radicals. Various instruments using different principles have been developed during the last decades to perform these measurements, including Matrix Isolation Electron Spin Resonance spectroscopy (MIESR: HO_2, RO_2) (Mihelcic et al., 2003, 1985), Laser-Induced Fluorescence (LIF-FAGE: HO_2, HO_2*; RO_xLIF: HO_2, HO_2+RO_2) (Stevens et al., 1994; Fuchs et al., 2008; Dusanter et al., 2009; Faloona et al., 2004), Chemical Ionisation Mass Spectrometry using PERCIMS (HO_2, HO_2+RO_2) (Edwards et al., 2003; Hornbrook et al., 2011; Kukui et al., 2008) and Br-CIMS (HO_2) (Sanchez et al., 2016), PEroxy Radical Chemical Amplification (PERCA: HO_2+RO_2) (Cantrell et al., 1984; Hernández et al., 2001; Kartal et al., 2010; Liu et al., 2009; Wood and Charest, 2014), and the more recent Ethane based CHemical AMPlification (ECHAMP) technique (Wood et al., 2017).

PERCA is an indirect measurement method pioneered by Cantrell and Stedman (Cantrell et al., 1984), which measures the sum of peroxy radicals continuously with high sensitivity. Ambient air is sampled in a reactor where each peroxy radical will lead to the formation of several NO_2 molecules via chain reactions after the addition of high concentrations of NO and CO. Once all the peroxy radicals have been consumed, NO_2 is measured by a suitable detector based on luminol chemiluminescence (Clemitshaw et al., 1997), LIF (Sadanaga et al., 2004), cavity ring-down spectroscopy (CRDS) (Horstjann et al., 2014; Liu et al., 2009; Liu and Zhang, 2014) or cavity attenuated phase-shift spectroscopy (CAPS) (Wood and Charest, 2014).

The amplification chemistry resulting from the addition of NO and CO is shown below:

$$\boldsymbol{RO_2 + NO \rightarrow RO + NO_2} \quad \text{R1a}$$

$$RO_2 + NO + M \rightarrow RONO_2 + M \quad \text{R1b}$$

$$RO + O_2 \rightarrow R_{-H}O + HO_2 \quad \text{R2}$$

$$RO + NO + M \rightarrow RONO + M \quad \text{R3}$$

$$HO_2 + NO \rightarrow OH + NO_2 \quad \text{R4a}$$

$$HO_2 + NO + M \rightarrow HNO_3 + M \quad \text{R4b}$$

$$HO_2 + wall \rightarrow loss \quad \text{R5}$$

$$OH + CO\ (+O_2) \rightarrow \cdots \rightarrow CO_2 + HO_2 \quad \text{R6}$$

$$OH + NO + M \rightarrow HONO + M \quad \text{R7}$$

$$OH + wall \rightarrow loss \quad \text{R8}$$

With the addition of a large amount of NO in the sampling reactor, RO_2 radicals are converted into HO_2 through the formation of an alkoxyl radical (RO) (R1a & R2). This HO_2, together with the sampled HO_2, are converted into OH (R4a). During this process, several molecules of NO_2 are produced, depending on the competition between propagation (R1a, R2, R4a) and termination (R1b, R3, R4b, R5) reactions. Then, several fast interconversions between OH and HO_2 occurs through the reaction of OH with CO (R6) and the reaction of HO_2 with NO (R4a), leading to the formation of additional molecules of NO_2. The number of NO_2 molecules formed during these interconversion steps is called chain length (CL) and is limited by the competition occurring between propagation (R4a, R6) and termination (R4b, R5, R7, R8) reactions of both OH and HO_2. The CL is typically in the range of 100−200 under dry conditions (Clemitshaw et al., 1997; Sadanaga et al., 2004; Wood and Charest, 2014).

The most problematic issue concerning PERCA instruments is the chain length dependence on Relative Humidity (RH), which translates into a RH-dependent sensitivity (Mihele and Hastie, 2000, 1998; Sadanaga et al., 2004). The chain length decreases monotonically with RH, likely due to increased losses of radicals on wet surfaces (Mihele et al., 1999; Miyazaki et al., 2010) and an increase in the HNO_3 yield in reaction R4b. The latter may involve H_2O dimers or the formation of a HO_2-H_2O complex (Reichert et al., 2003). The effect of water vapor on the branching ratio of R4b was investigated by Butkovskaya et al. (Butkovskaya et al., 2009) who reported a linear increase of the HNO_3 yield with RH, with an enhancement factor of about 8 at 50% RH. A rate constant for the reaction between HO_2-H_2O and NO producing HNO_3 was estimated from this work and was found to be 40 times faster than the rate constant for HO_2+NO→HNO_3. This water vapor enhancement of the gas-phase termination rate of HO_2 may play an important role in the reduction of the chain length.

The amplification chemistry used in ECHAMP relies on the addition of ethane (C_2H_6) instead of CO as proposed by Wood et al. (Wood et al., 2017). The advantages reported by the authors are a lower sensitivity of the CL to relative humidity and a safer use of the instrument in confined areas since ethane is less toxic than CO. The chemical reactions describing the radical cycling when ethane and NO are added

in the reactor are the same as above (R1-R8), with the exception than R6 is replaced by the set of reactions shown below:

$$OH + C_2H_6\ (+O_2) \rightarrow \cdots \rightarrow H_2O + C_2H_5O_2 \quad \text{R9}$$

$$C_2H_5O_2 + NO \rightarrow C_2H_5O + NO_2 \quad \text{R10a}$$

$$C_2H_5O_2 + NO \rightarrow C_2H_5ONO_2 \quad \text{R10b}$$

$$C_2H_5O + O_2 \rightarrow CH_3CHO + HO_2 \quad \text{R11}$$

$$C_2H_5O + NO \rightarrow C_2H_5ONO \quad \text{R12}$$

Ethane reacts with OH to produce an ethylperoxyl radical ($C_2H_5O_2$) (R9), which then (i) propagates to HO_2 (R10a, R11) through the formation of an alkoxyl radical (C_2H_5O) or (ii) terminates through the formation of organic nitrate (R10b) or nitrite (R12) compounds. Since the interconversion steps between OH and HO_2 go through the formation of $C_2H_5O_2$ and C_2H_5O, the additional loss of radicals (R10b, R12) will lead to a lower CL than for the PERCA approach. It has been shown that this amplification chemistry leads to chain lengths ranging from 25-30 (RH of 1-10%) (Wood et al., 2017). However, if heterogeneous losses of peroxy radicals on the reactor wall contribute significantly to the total termination rate of radicals in the reactor, the CL for ECHAMP should be less sensitive to RH compared to PERCA since $C_2H_5O_2$ exhibits a lower loss rate on wet surfaces than HO_2 (Mihele et al., 1999). For example, Mihele et al. (1999) reported a wall loss rate on Teflon (PFA) of 2.8 ± 0.2 s^{-1} for HO_2 and 0.8 ± 0.1 s^{-1} for $C_2H_5O_2$ under dry conditions and showed that the HO_2 loss rate increases with RH in contrast to organic peroxy radicals. This observation was also confirmed by Miyazaki et al. (2010) who reported a 6-fold higher removal efficiency of HO_2 on Teflon (PFA) surfaces compared to organic peroxy radicals.

PERCA and ECHAMP instruments used in the field are based on dual-channel sampling systems (Liu et al., 2009; Horstjann et al., 2014; Wood et al., 2017; Kartal et al., 2010) to simultaneously quantify NO_2 under two measurement modes (background and amplified modes). In the background mode, NO and N_2 are injected at the entrance of the sampling reactor and CO or ethane (same volumetric flow rate than N_2) is injected at the exit of the reactor once all the radicals have been terminated. Since CO or ethane are not added together with NO, there is no amplification chemistry. The NO_2 mixing ratio exiting the reactor is the sum of ambient NO_2, a fraction of O_3 titrated by NO, and the amount of NO_2 produced during the first peroxy radical-to-OH conversion step (R1a, R2, R4a). For the amplification mode, CO or ethane is

injected at the entrance of the reactor while N_2 is injected at the exit, allowing the amplification chemistry of peroxy radicals to take place. The mixing ratio of NO_2 at the exit of the reactor is the sum of that observed during the background mode and the NO_2 produced during amplification. The amount of NO_2 generated during amplification (ΔNO_2) is inferred from the difference between the amplification and background modes.

It is important to note that these instruments will amplify all radicals that can propagate to HO_2, including RO_2 but also OH and RO. While the measurements of a chemical amplifier represent the sum of RO_x, tropospheric concentrations of OH and RO are ~200-1000 times lower than those of HO_2 and RO_2 and the measurements are thus considered as being the sum of HO_2 and RO_2.

The total mixing ratio of peroxy radicals calculated from the amount of NO_2 produced during the amplification stage (ΔNO_2) and the CL is retrieved as shown in Eq. 1.

$$[\boldsymbol{HO_2}] + \sum[\boldsymbol{RO_2}] = \Delta \boldsymbol{NO_2/CL} \qquad \text{Eq. 1}$$

Quantifying the sum of peroxy radicals from Eq. 1 requires calibrating the CL by generating a known concentration of HO_2 or another peroxy radical. The CL is usually only calibrated for a few radicals by generating a known concentration of methyl peroxy (CH_3O_2) and peroxyacetyl ($CH_3C(O)O_2$), both being simultaneously produced from the photolysis of acetone at 254 nm (Miyazaki et al., 2010; Wood and Charest, 2014). Another method used to calibrate the chain length is based on the generation of CH_3O_2 from the photolysis of methyl iodide (CH_3I) in air at 254 nm (Clemitshaw et al., 1997; Green et al., 2006).

This publication reports the construction of a dual-channel chemical amplifier for ambient measurements of peroxy radicals using both the PERCA (CO/NO) and ECHAMP (ethane/NO) approaches. The main objective was to improve our understanding of these two approaches, which will ultimately provide a better assessment of uncertainties associated to chemical amplifiers' measurements. In this context, optimal operating conditions were identified for each approach and experimental observations were compared to box-model simulations to gauge our understanding of the radical amplification chemistry. The instrument was calibrated using a large range of peroxy radicals, including HO_2 and organic peroxy radicals formed during the OH-oxidation of alkanes, alkenes, aromatics and oxygenated VOCs. These experiments allowed investigating whether the change in CL observed experimentally is consistent with the formation yield of organic nitrate ($RONO_2$) or nitrite (RONO) species reported in the literature for

each tested radical. Finally, ambient measurements are reported to illustrate the performances of this instrument.

2 Experimental Section

2.1 Description of the chemical amplifier

A schematic of the apparatus built at IMT Lille Douai is shown in Figure 1. It consists of two sampling reactors operated in amplification and background modes, two monitors to simultaneously measure NO_2 at the exit of the reactors, and two sets of solenoid valves to switch (i) between background and amplification modes in each reactor (SV1a, SV1b, SV2a, SV2b) and (ii) the sampling of the NO_2 monitors between the two reactors (SV3, SV4) as further described below for the measurement sequence.

Ambient air is sampled into two PerFluoroAlkoxy (PFA) reactors (0.635 cm o.d. × 60 cm length, thickness 0.08 cm) using two PFA inlets (0.635 cm o.d. × 1.5 cm length) at a total flow rate of approximately 800 cm^3 min^{-1}. The inlets and the reactors are connected together using home-made 3D printed nylon couplers (Figure S1), allowing to add and mix the reagent gases with the sampled air. The reagent gases are mixed with ambient air through two circular channels (2 mm apart) between the sampling inlet and the reactor, each channel being characterized by 5 radial injection holes. This design was adopted to improve the mixing between ambient air and the reagents. All flow rates are regulated by mass flow controllers.

For the amplification channel, NO (84 SCCM-PERCA, 14 SCCM-ECHAMP, 50 ppm in N_2) and CO (80 SCCM, 100%) or ethane (50 SCCM, 30% in N_2) are added upstream the reactor via the nylon injector, while a flow of nitrogen (equivalent to the CO or ethane flow rate) is added downstream the reactor, approximately 60 cm (0.9 s residence time) after the initial injection of CO (or ethane). For the background mode, N_2 is added upstream while CO (or ethane) is added downstream. Four solenoid valves (SV1a, SV1b, SV2a, SV2b) allow switching the addition of CO (or ethane) and nitrogen between the downstream and upstream injection ports, to change the measurement mode in each reactor. Flow rates of CO (or ethane), NO and N_2 have been optimized to get the highest CL for both amplification chemistries and are discussed in the results section (Table 2). At the exit of the reactors, air exempt of RO_x radicals is transported through additional 6-m long pieces of PFA tubing (0.635 cm o.d.) to the NO_2 monitors at a flow rate of 800 cm^3 min^{-1}.

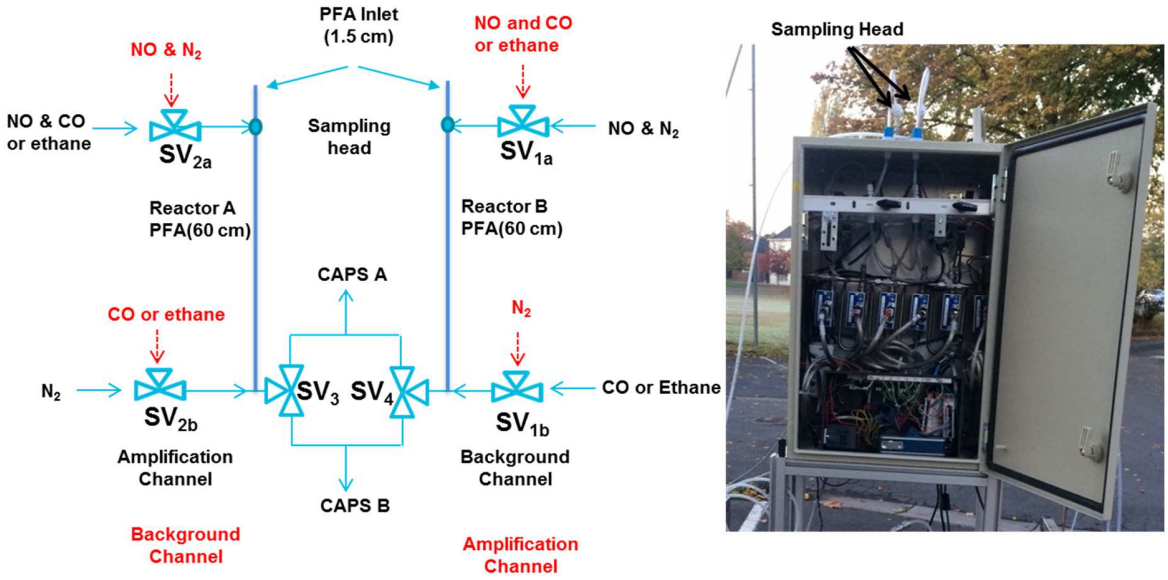

Figure 1: Schematic of the IMT Lille Douai PERCA instrument

High sensitivity CAPS (Cavity Attenuated Phase Shift) monitors from AERODYNE Research Inc. were coupled to the reactors to quantify NO_2. For the monitors used in this work, air is sampled through a nafion dryer and enters an 82 cm^3 stainless steel absorption cell held at 27 °C, consisting of two high reflectivity mirrors (R ~ 99.99%). The photons provided to the absorption cell are emitted by a blue light-emitting diode (LED). The light exiting the cell passes through a bandpass filter centered at 450 nm and is detected by a vacuum photodiode. The NO_2 concentration is derived from the phase-shift observed in the detected signal, which is proportional to the amount of NO_2.

All reagent gases were found to generate a spurious signal in the CAPS monitors. The addition of 1-6 ppm of NO (99.995% purity) in the reactors leads to several ppb of NO_2 due to contamination of the NO mixture by NO_2 and a potential conversion of NO into NO_2 in the lines and mass flow controllers. To reduce this spurious signal, the NO reagent gas was purified using an inline chemical filter made of iron(II) sulfate heptahydrate ($FeSO_4.7H_2O$, Fisher scientific). This filter was found to be very efficient with less than 0.2 ppb of NO_2 remaining in the reactor after the addition of 1 ppm of NO. The addition of 10% CO and 2% ethane in the reactors led to a spurious signal equivalent to approximately 1.5 and 3 ppb of NO_2. This signal was found to be proportional to the reagent concentration and is thought to be due to light scattering since these species do not absorb at 450 nm. A lowest signal observed for CO seems

consistent with lower scattering cross-sections reported in the literature for this species compared to alkanes (Sneep and Ubachs, 2005; Sutton and Driscoll, 2004).

A sequence of 4 steps of 90-s measurements spanning a 6-min period is required to measure a concentration of peroxy radicals (Figure S2): (1) NO_2 is measured from each reactor, a reactor being operated in background mode and the other reactor in amplification mode; (2) the CAPS sampling inlets are switched between the two reactors; (3) both the measurement mode and the CAPS sampling are switched between the 2 reactors; (4) the CAPS sampling inlets are switched. All NO_2 measurements performed under amplified conditions are averaged together and all measurements performed under background conditions are also averaged together. Only the last 70-s of each NO_2 measurement step are used in the averaging process to calculate ΔNO_2 (see S2). This sequence of steps is necessary to cancel out any bias in ΔNO_2 arising from (i) a drift in monitors' zeros and (ii) slightly different behaviors of the 2 reactors (spurious NO_2 signals from reagents, O_3 titration by NO, wall losses of O_3…).

All compressed gas cylinders used in this study were provided commercially: CO (100%, Air Liquide, France), ethane (30±2% in N_2, Linde Co.), NO (50 ppm in N_2, Air Liquide), N_2 (Messer, purity >99.9999%). Volatile organic compounds were purchased from Sigma Aldrich with a purity better than 99%.

2.2 Calibration of the Chain Length (CL)

As discussed in the introduction section, the CL can be quantified from Eq. 1 when the instrument samples air containing a known concentration of peroxy radicals. Peroxy radicals were generated in this study through the photolysis of water-vapor at 184.9 nm in a turbulent flow tube, creating an equimolar mixture of OH and HO_2 (Reactions R13-R14). This method is commonly used to calibrate field measurements of OH and HO_2 performed by LIF-FAGE instruments (Dusanter et al., 2008).

$$H_2O + h\nu\ (\lambda = 184.9nm) \rightarrow OH + H \qquad \text{R13}$$

$$H + O_2 + M \rightarrow HO_2 + M \qquad \text{R14}$$

In this study, OH was quantitatively converted into HO_2 by adding CO in the calibrator as shown in R6 or by adding a volatile organic compound (VOC) to generate a mixture of HO_2 and RO_2 radicals (Lew et al., 2018). For instance, isoprene (C_5H_8) is added inside the calibrator to convert OH into an organic peroxy

radical mixture of $C_5H_8(OH)O_2$ isomers. The CO and VOC concentrations were set to convert approximately 99% of OH in less than 2 ms, ensuring a negligible OH loss on the calibrator inner surface. Diluted mixtures of each targeted VOC (Table 1) were prepared by injecting the pure compound into 18 liters of zero air (6-L stainless steel canisters at 3 bars). A flow rate of 2.5 SCCM (Standard Cubic Centimeter per Minute) of the diluted CO or VOC mixtures was mixed with 35 SLPM (Standard Liter per Minute) of dry or humid zero air in the calibrator using mass flow controllers. RH was varied in the range 10-90% (T=24±2°C) to produce peroxy radical concentrations within the range 2×10^9-3×10^{10} cm^{-3}.

Series of calibration experiments were performed using CO and all the VOCs reported in Table 1. When CO is used, only HO_2 exits the calibrator and the measured CL is characteristic of only one peroxy radical. This CL is defined as $CL_{(HO2)}$ in the following. However, when a VOC is added in the calibrator, an apparent CL is measured for a mixture of HO_2 and RO_2 radicals. Rearranging Eq. 1 leads to Eq. 2 for the calculation of this CL, which will depend on the generated RO_2 radical.

$$CL = \Delta NO_2/([HO_2] + [RO_2]) \quad \text{Eq.2}$$

The radical concentrations at the exit of the calibrator are inferred from Eqs 3-4.

$$[HO_2] = (1 + X) \times [H_2O] \times \sigma_{water} \times \emptyset_{OH+H} \times (F \times t) \quad \text{Eq. 3}$$

$$[RO_2] = (1 - X) \times [H_2O] \times \sigma_{water} \times \emptyset_{OH+H} \times (F \times t) \quad \text{Eq. 4}$$

Here, HO_2 and RO_2 concentrations are calculated from the water concentration inside the calibrator, $[H_2O]$, its absorption cross-section at 184.9 nm, σ_{water}, the photo dissociation quantum yield, Φ_{OH+H}, the photon flux, F, and the photolysis duration, t. The terms $(1+X)$ and $(1-X)$ account for the non-unity RO_2 yield observed for some VOCs (Table 1), X being the prompt yield of HO_2, which allows accounting for its direct formation together with the formation of RO_2 radicals from RH+OH reactions. The absorption cross section for H_2O and quantum yield for OH+H reported in several studies are 7.14×10^{-20} cm^2 $molecule^{-1}$ (Cantrell et al., 1997; Creasey et al., 2000) and unity, respectively. The product (F×t) is measured experimentally by ozone actinometry using Eq. 5, where $[O_2]$ is the oxygen concentration, σ_{O2} the oxygen absorption cross section at 184.9 nm (1.21×10^{-20} cm^{-2}) (Dusanter et al., 2008), and $[O_3]$ the ozone concentration produced in the calibration cell. The latter has to be measured during a calibration experiment.

$$(F \times t) = [O_3]/\left(2 \times [O_2] \times \sigma_{O_2}\right) \quad \text{Eq.5}$$

During a calibration experiment [O_3] was measured as NO_2 by CAPS after titration by NO in one of the reactors operated in background mode, keeping NO at the same mixing ratio than used for PERCA or ECHAMP measurements of peroxy radicals. For this measurement, dry zero air was flown in the calibrator and the mercury lamp was switched ON and OFF several times to determine [O_3] by subtraction. Ozone concentrations were in the range of 2.5-3.0 ppb. [H_2O] was measured by a LI-COR 840A based on infrared absorption and calibrated versus a dew-point hygrometer (Mitchell S8000). The CAPS instruments were calibrated with an NO_2 standard mixture at 190 ± 3 ppb (2σ) certified by LNE (French National Metrology Institute).

The accuracy of the calibrated CL (Eq. 2) depends on the uncertainty of both the measured ΔNO_2 and the generated peroxy radical concentration. The precision on ΔNO_2 can be neglected since the use of large radical concentrations during calibration experiments leads to a negligible random error associated to the quantification of the NO_2 signal. If CO is added in the calibrator to only produce HO_2, the accuracy (2σ) on ΔNO_2 (1.5%) is much lower than the accuracy on the generated peroxy radical concentration of 31% (2σ) as reported by Dusanter et al. (2008) for the same calibrator ran under similar operating conditions. A propagation in quadrature leads to a total accuracy of 31% (2σ) for the CL.

The apparent chain length for individual RO_2 radicals, $CL_{(RO2)}$, was computed from Eq. 6. ΔNO_2 is the amount of NO_2 produced when both HO_2 and RO_2 radicals are sampled by the instrument, $CL_{(HO2)}$ is determined during a calibration experiment using CO, and both HO_2 and RO_2 concentrations are calculated from Eqs. 3-5.

$$CL_{(RO_2)} = \left(\Delta NO_2 - CL_{(HO_2)} \times [HO_2]\right)/[RO_2] \quad \text{Eq. 6}$$

Direct photolysis of the parent VOCs was investigated during these calibration experiments using dry conditions (RH< 1%). The fraction of ΔNO_2 due to radicals produced by VOC photolysis was quantified for each experiment and was subtracted from ΔNO_2 to calculate $CL_{(RO2)}$ from Eq. 6. Table 1 reports the fraction of radicals produced by direct photolysis for each VOC. The amount of NO_2 produced by the radicals generated through the photolysis of VOCs was always lower than 7% of ΔNO_2 (photolysis of VOCs + water photolysis), with the exception of vinylacetate (14%).

The difference between $CL_{(HO2)}$ and the apparent $CL_{(RO2)}$ should only depends on RO_2-to-HO_2 propagation reactions (R1-R3), which can be factored into a RO_2-to-HO_2 transmission term as shown in Eq. 7, $T_{(RO2)}$ being the fraction of RO_2 radicals propagated to HO_2.

$$CL_{(RO_2)} = CL_{(HO_2)} \times T_{(RO_2)} \quad \text{Eq. 7}$$

2.3 Box modeling of the amplification chemistry

The Master Chemical Mechanism (MCM) v3.2 and the F0AM model (Framework for 0-D Modeling) (Wolfe et al., 2016) were used to simulate both the amplification and background modes under different operating conditions of reagents and humidity. A radical wall loss for HO_2 was added in the chemical mechanism with a first order loss rate parameterized from experimental measurements of radical losses in the PFA reactors (supplementary material S3). In addition, since MCM does not include RO+NO reactions, which are not important for atmospheric chemistry but essential for the chemistry occurring in the chemical amplifier, the reaction of C_2H_5O with NO leading to the formation of C_2H_5ONO was added using a rate constant of 4.4×10^{-11} cm^3 $molecule^{-1}$ s^{-1} (Atkinson et al. 1997). MCM does not include the formation of HNO_3 from the HO_2+NO reaction (Butkovskaya et al., 2009, 2007)which is thought to occur through the formation of the $HO_2.H_2O$ complex. A branching ratio for the formation of HNO_3 was included in the MCM to perform sensitivity tests. The branching ratio for this reaction ($k_{HO_2+NO\rightarrow HNO_3}/k_{HO_2+NO\rightarrow OH+NO_2}$) was considered to be 0.5% under dry conditions (Butkovskaya et al., 2007) and dependent on RH with an amplification factor of 8 at 50% RH (Butkovskaya et al., 2009). Sensitivity tests were performed using (1) a water-independent branching ratio of 0.5% (HNO_3/dry in Figures 2-4), (2) a linear parameterization of the ratio on RH leading to a value of 0.5% under dry conditions and a value 8 time higher at 50% RH (HNO_3/RH_dep in Figures 2-4), and (3) a parameterization leading to half the water-dependence reported by Butkovskaya et al. (2009) (HNO_3/adj_RH_dep in Figures 2-4). Uncertainties on the later simulations (dotted lines in Figures 2-4) were derived as reported in Wood et al. (2007) assuming an error of 25% on the branching ratio under dry conditions and an additional error of 28% associated to the humidity dependence of this ratio.

The model was used to calculate the NO_2 concentration at the exit of each reactor for an initial concentration of HO_2 at the inlet similar to those generated during calibration experiments of the CL. The simulations were run for 5-s of reaction time and the model output of NO_2 at 2-s of reaction time was used to calculate the modeled CL using Eq. 2. These simulations have shown that the amount of NO_2 produced

from the radical amplification chemistry levels off at approximately 0.5-s of reaction time, e.g. NO_2(0.5-s)/NO_2(5-s)>97.7%.

Table 1 Summary table of targeted VOCs.

VOC	*Concentration in calibrator (molecules cm^{-3})*	*OH rate constant* ($cm^3 molecule^{-1} s^{-1}$)*	*HO_2 yield⁂ VOC+OH reactions (X) (%)*	ΔNO_2(VOC photolysis) / ΔNO_2 (VOC photolysis+water photolysis) (%)
Isoprene	6.2×10^{12}	1.0×10^{-10}	6	1.7
Limonene	3.7×10^{12}	1.7×10^{-10} ϕ	-	1.9
m-xylene	2.5×10^{13}	2.3×10^{-11} **	45	0.5
β-pinene	7.7×10^{12}	7.8×10^{-11}	-	3.3
Methylvinylketone	3.5×10^{13}	2.0×10^{-11}	-	3.2
Acetaldehyde	3.8×10^{13}	1.5×10^{-11}	-	0.1
Pentane	1.6×10^{14}	3.8×10^{-12} ∞	-	0.3
3-methylpentane	1.2×10^{14}	5.2×10^{-12} ∞	-	-
Cyclohexane	8.8×10^{13}	7.0×10^{-12} ∞	-	-
Toluene	1.0×10^{14}	5.9×10^{-12} **	28	0.7
Vinylacetate	4.8×10^{13}	1.3×10^{-11} ***	-	14
1-pentene	2.1×10^{13}	3.1×10^{-11} "	-	5.6
Cyclopentene	1.1×10^{13}	6.7×10^{-11} "	-	6.6

*(Atkinson et al., 2006); **(Calvert et al., 2011)CAC ***(Teruel et al., 2006); "(Atkinson, 1986); ∞(Atkinson, 2003); ϕ (Braure et al., 2014); ⁂ HO_2 yields from MCM V3.2

3 Results & Discussion

This section reports a series of characterization and optimization experiments using both PERCA (CO/NO) and ECHAMP (ethane/NO) approaches. The impact of relative humidity on the chain length is investigated for each approach using operating conditions leading to the highest sensitivity. In addition, a

337 comparison of measured CL to values inferred from box modeling is used to test our understanding of
338 each amplification chemistry. The differences observed in CL when calibrating the chemical amplifier
339 with different RO_2 radicals are investigated and contrasted to differences expected from the formation of
340 organic nitrate (R1b) and nitrite (R3) species. Finally, field measurements are presented to illustrate the
341 performances of this instrument.

342 ## 3.1 Gas Reagents Optimization

343 A mixture of HO_2 and organic peroxy radicals was generated by adding isoprene in the calibrator as
344 described in the experimental section. The dependence of the measured (markers) and modeled (lines)
345 chain lengths on reagent gases at 50% RH are shown in Figures 2 and 3. For PERCA (Figure 2), CO and
346 NO were varied in the range 0.6-20% and 0.3-12.5 ppm, respectively. Figures 2a shows that both
347 experimental and modeled CL increase with the addition of NO up to 5-6 ppm at a constant CO mixing
348 ratio of 4.5%. When NO is increased over 6 ppm, the CL starts decreasing due to a faster increase of the
349 OH + NO (R7) reaction rate compared to HO_2 + NO (R4a). Figure 2b shows that when CO is varied at a
350 constant NO mixing ratio of 6 ppm, a plateau seems to be reached at CO mixing ratios higher than 10%.
351 Other studies have shown similar results with a plateau reached at approximately 7% (Clemitshaw et al.,
352 1997; Kartal et al., 2010; Sadanaga et al., 2004), 10% (Sadanaga et al., 2004) and 8.7% CO (Wood et al.,
353 2014) for NO mixing ratios of 3, 3 and 3.3 ppm, respectively. The difference between these operating
354 conditions that are optimized to get the largest CL may be due to the use of different materials to build the
355 reactors and different reactor designs, which led to different wall losses of radicals.

356 While the relative NO- and CO-dependencies of the CL are well described by the different models, Figure
357 2b shows that experimental CL values are lower than modelled values by approximately a factor of 2
358 when the base MCM simulation is considered (see section 2.3, red line), with maximum values around 55
359 and 120 at 10% CO, respectively. The simulation accounting for the formation of HNO_3 from HO_2+NO
360 with a water-independent branching ratio of 0.5% (HNO_3/dry, grey line) is in better agreement with the
361 measured CL values, with a small overestimation of the model by approximately 15-25%. Implementing
362 the water-enhancement of the HNO_3 yield reported in the literature (see section 2.3) leads to a severe
363 model underestimation by a factor of approximately 2. This issue is further discussed for the 2
364 amplification chemistries below.

365

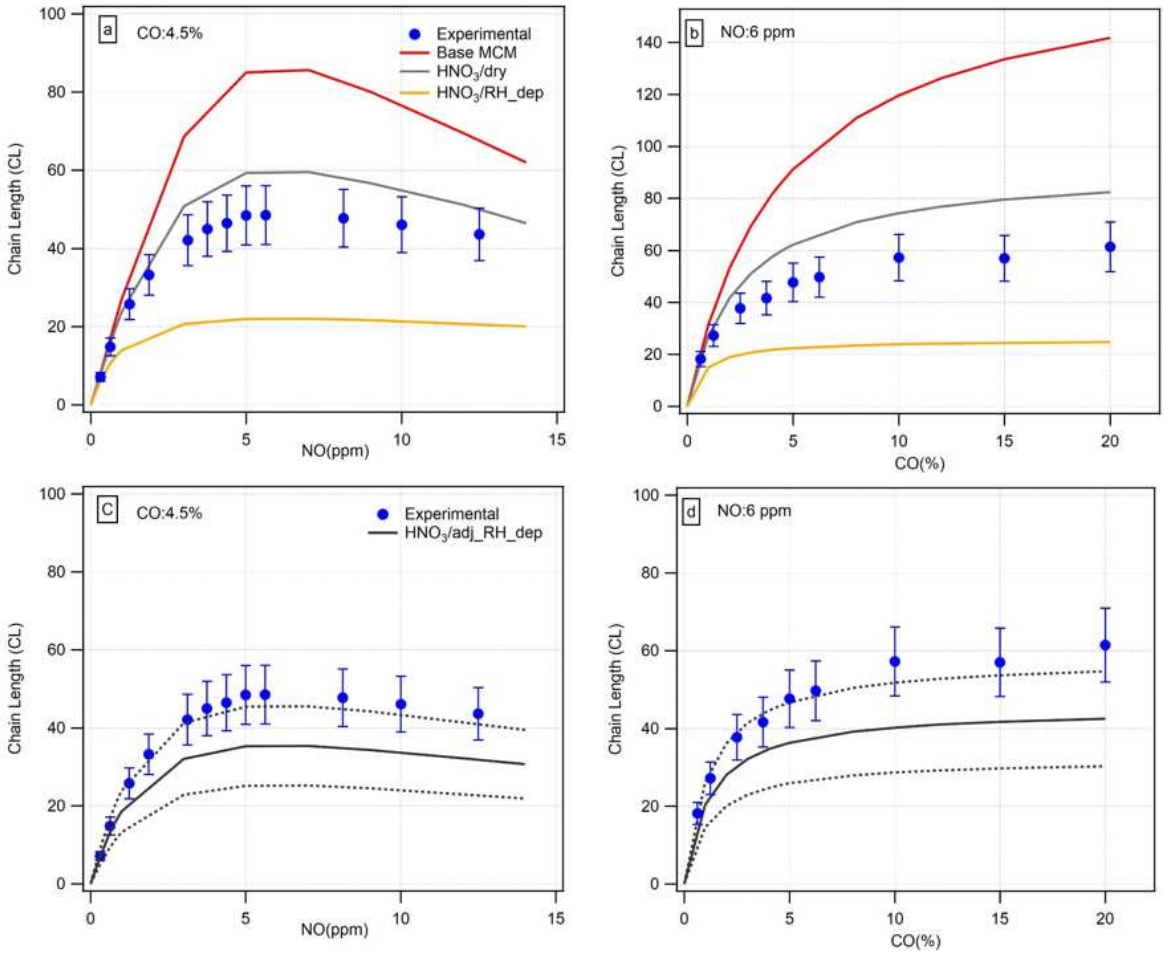

Figures 2: Chain length dependences on reagent gases for the PERCA (CO/NO) approach. Experimental and modeled values are shown as markers and lines, respectively. Experiments were performed at ambient temperature (23°C) and 50% RH. Uncertainty on experimental values are 1σ. Panels c,d: dotted lines are uncertainty on modelled values. See section 2.3 for the modeling scenarios.

For the ECHAMP approach, the 2 reagents were varied on a smaller range of concentrations, c.a. 0.4-6.0% for ethane and 0.2-3.1 ppm for NO. Figure 3 displays the dependence of both experimental and modeled CL on NO (panel a) and ethane (panel b). The relative dependence on both reagents (curve shape) is similar to that observed for PERCA with optimum CL values for NO and ethane mixing ratios of 0.9 ppm and 2.1%, respectively. These optimum CL values are similar to values reported by Wood et al.

(Wood et al., 2017) using 2.3% ethane and 1 ppm NO, respectively. The highest CL is approximately 3 times lower than for the PERCA approach, due to additional losses of radicals through the formation of nitrate (R1b) and nitrite (R3) compounds during the radical amplification stage. Similarly to the PERCA approach, CL values simulated by the base MCM model are systematically higher than experimental values by a factor of approximately 2. In addition, as clearly seen in Figure 3c, the shape of the experimental trace is not well reproduced by the model with a peak in CL at higher NO for the model. Implementing the formation of HNO_3 from HO_2+NO using the water-independent branching ratio has a much lower impact on the modelled CL values than for PERCA with a decrease of the CL by only 5-7%. This lower impact is due to a smaller contribution of this additional loss process to the total loss of radicals in the reactor (larger total loss rate compared to PERCA due to organic nitrite and nitrate formation from R3 and R1b, respectively). Using the water-dependent parameterization of the yield brings the modeled values in much better agreement with the measurements, which contrasts to that observed for the PERCA approach.

Additional simulations were performed for both PERCA and ECHAMP in order to see whether a smaller water-enhancement of the HNO_3 formation yield could reconcile the model/measurement comparison for the two amplification chemistries when uncertainties on modeled and measured CL values are considered. As shown in Figures 2 and 3 (panels c and d), simulated CL values considering an enhancement factor of 4 at 50% RH (HNO_3/adj_RH_dep) would lead to modeled CL values that are within uncertainties with experimental measurements. Looking at each amplification chemistry separately would lead to the conclusion that the measured CL values and dependences on reagent gases could be relatively well reproduced if the water-dependence reported by only one study in the literature is overestimated by a factor 2. However, a systematic error on the parameterization of the HNO_3 yield in the model should lead to a systematic deviation from the measurements (either positive or negative) for both comparisons (PERCA and ECHAMP). It is clear that while the additional loss of radicals due to HNO_3 formation is important for both PERCA and ECHAMP, the uncertainty related to its parameterization cannot fully account for the model/experiment disagreement observed in this study (model underestimation for PERCA and overestimation for ECHAMP) and additional work is needed to improve our understanding of these amplification chemistries.

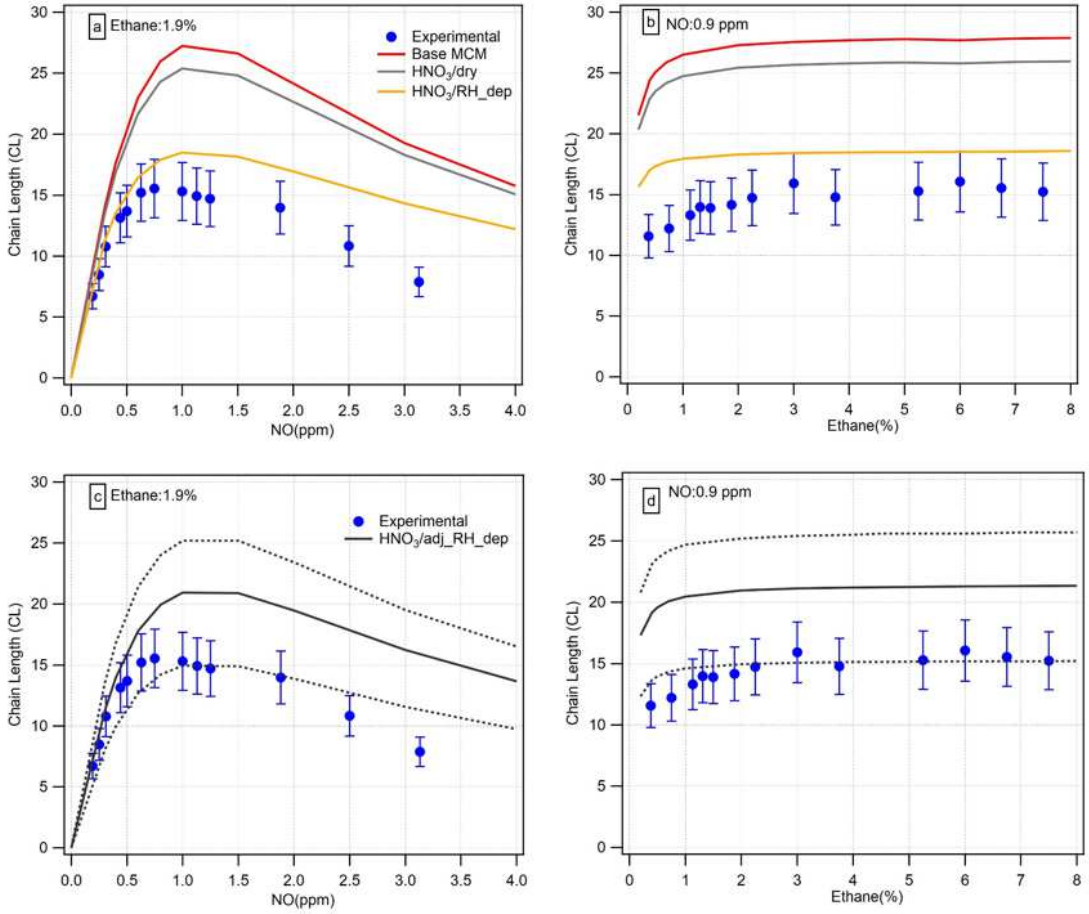

Figures3: Chain length dependences on reagent gases for the ECHAMP (ethane/NO) approach. Experimental and modeled values are shown as markers and lines, respectively. Experiments were performed at ambient temperature (23°C) and 50% RH. Uncertainty on experimental values are 1σ. Panels c,d: dotted lines are uncertainty on modelled values. See section 2.3 for the modeling scenarios.

It is interesting to note that a large impact of radical losses in the inlet of the chemical amplifier on this model/measurement comparison was ruled out. As mentioned in the experimental section, first order wall loss rates of HO_2 and $CH_3CH_2O_2$ were measured experimentally at different RH and were found to be 7.1 s^{-1} and lower than 1 s^{-1}, respectively, at 50% RH. Based on the residence time in the PFA inlet (22 ms) and the first order loss rate observed for HO_2, a conservative upper limit of 11% is estimated for the amount of peroxy radicals lost on the wall. In addition, increasing the total flow rate inside the inlet by a factor of 2

did not significantly impact the measured CL values. It is also interesting to note that setting the wall loss of HO_2 to zero in the base MCM model leads to an increase of the modeled chain length by a factor of 2, indicating that a modification of the reactor geometry to reduce the surface-to-volume ratio and the use of a more hydrophobic material to build the reactors may help increasing the experimental CL and hence the sensitivity of the instrument.

Table.2 Operating conditions for the PERCA and ECHAMP approaches

Parameter	Value
PFA reactor PFA inlet	Length: 60 cm, Outer diameter: 0.635 cm Length:1.5 cm, Outer diameter: 0.635 cm
Sampling flow rate	Approx. 800 SCCM
Reactor residence time Inlet residence time	0.9 s 22 ms
ECHAMP approach (Ethane/NO)	
NO	0.9 ppm
Ethane	2.1%
Experimental CL (50% RH) Modeled CL (50% RH)	15 28
PERCA approach (CO/NO)	
NO	6 ppm
CO	10%
Experimental CL (50% RH) Modeled CL (50% RH)	55 105

3.2 Linearity of the chemical amplifier response (ΔNO_2) with HO_2

The linearity was investigated using the ECHAMP approach by adding CO in the calibrator to only produce HO_2. This experiment was performed using a calibrator equipped with a chemical N_2O filter located between the Hg lamp housing and the turbulent flow tube. The photon flux at 184.9 nm was varied over a factor of 40 by adjusting the concentration of N_2O inside the chemical filter, allowing to vary the HO_2 mixing ratios in the range 2-85 ppt (4.9×10^7-2.1×10^9 cm^{-3}) at a constant RH of 23%. These values encompass ambient concentrations usually observed during field campaigns.

Plotting ΔNO_2 versus HO_2 in Figure 4 indicates a good linearity over the tested range of concentrations. A linear regression exhibits a coefficient of determination (R^2) of 0.98 and a negligible intercept (not statistically significant at 1σ). The CL determined at 23% RH from the slope of this regression line is 24 ±

1 (1σ), which is larger than the CL reported in Figure 2d (approx. 15) under similar conditions of reagents at 50% RH, indicating a strong dependence of the CL with RH.

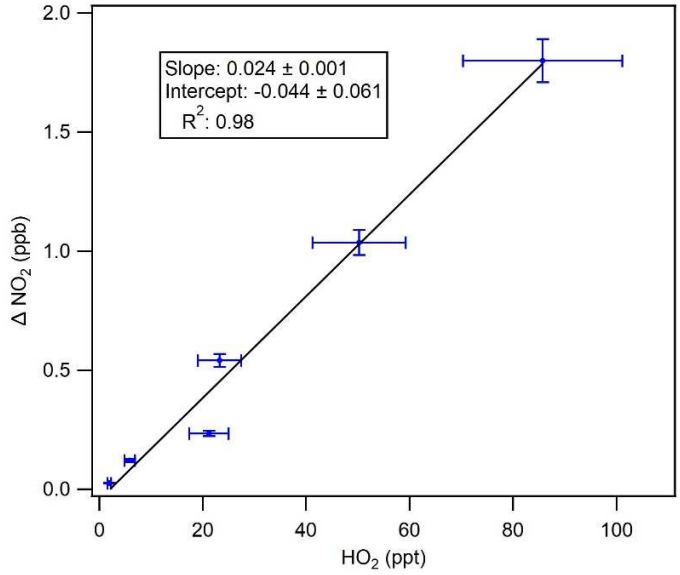

Figure 4: Scatter plot of ΔNO_2 with HO_2 for the ECHAMP approach. Experiments performed at a temperature of 23 °C and (23±2) % RH. The solid line represents the linear regression line; Error bars are 1σ uncertainty on NO_2 measurements and HO_2 generation. Errors on slope and intercept are 1σ.

3.3 Dependence of the CL on RH

The CL dependence on RH is considered as a major issue for chemical amplification techniques and was investigated for both ECHAMP and PERCA by varying RH in the range 10-85% during calibration experiments (isoprene added in the calibrator). As discussed in the introduction section, the CL decreases when humidity increases due to enhanced radical losses on wet surfaces and the potential impact of water dimers and $HO_2.H_2O$ complex on the gas-phase chemistry. To quantify this effect, the RH-dependence of both the experimental and modeled CL was investigated. Experimental (markers) and modeled (lines) CL for both amplification approaches are shown in Figure 5 as a function of RH. Operating conditions used during these experiments are reported in table 2 and experiments were performed at a temperature of 23±2°C.

In this figure, the experimental CL decreases with RH for both approaches, with a drop of about a factor of 3-4 between 10 and 70% RH. At 10% RH the CL for PERCA and ECHAMP are different by approximately a factor of 4. However, a larger RH-dependence of the CL is observed for PERCA, leading to a factor 3 of difference between the 2 approaches at 70% RH. These results are consistent with the work of Wood et al. (Wood et al., 2017) who reported a lower impact of RH for the ECHAMP technique.

The RH-dependence of the PERCA CL reported in this study exhibits a similar behavior to what was observed by Sadanaga et al. (Sadanaga et al., 2004) up to 60% RH, but seems steeper for RH values larger than 60%. This dependence is also consistent with a decrease by a factor of 2 at 40% RH compared to dry conditions reported in Wood et al. (2017). The modelled CL values displayed in panels a and b show that the simulations assuming a water-dependence of the HNO_3 formation yield adjusted at half the reported value can describe the RH-dependence of the measured CL within uncertainty, while the other simulations are in disagreement for both the absolute CL value and the RH-dependence.

For the ECHAMP approach, the RH-dependence is similar to observations reported in Wood et al. (2017), where the CL is lower by a factor of 1.5 at 40 % RH compared to dry conditions. The modelled CL displayed in panels c and d lead to similar conclusions than for the PERCA approach, where simulations based on a 2-fold lower-than-reported water-dependence for the HNO_3 formation yield are in agreement with the experimental observations within uncertainty up to 70% RH. These results are consistent with the simulation presented in the supplementary material of Wood et al. (2007).

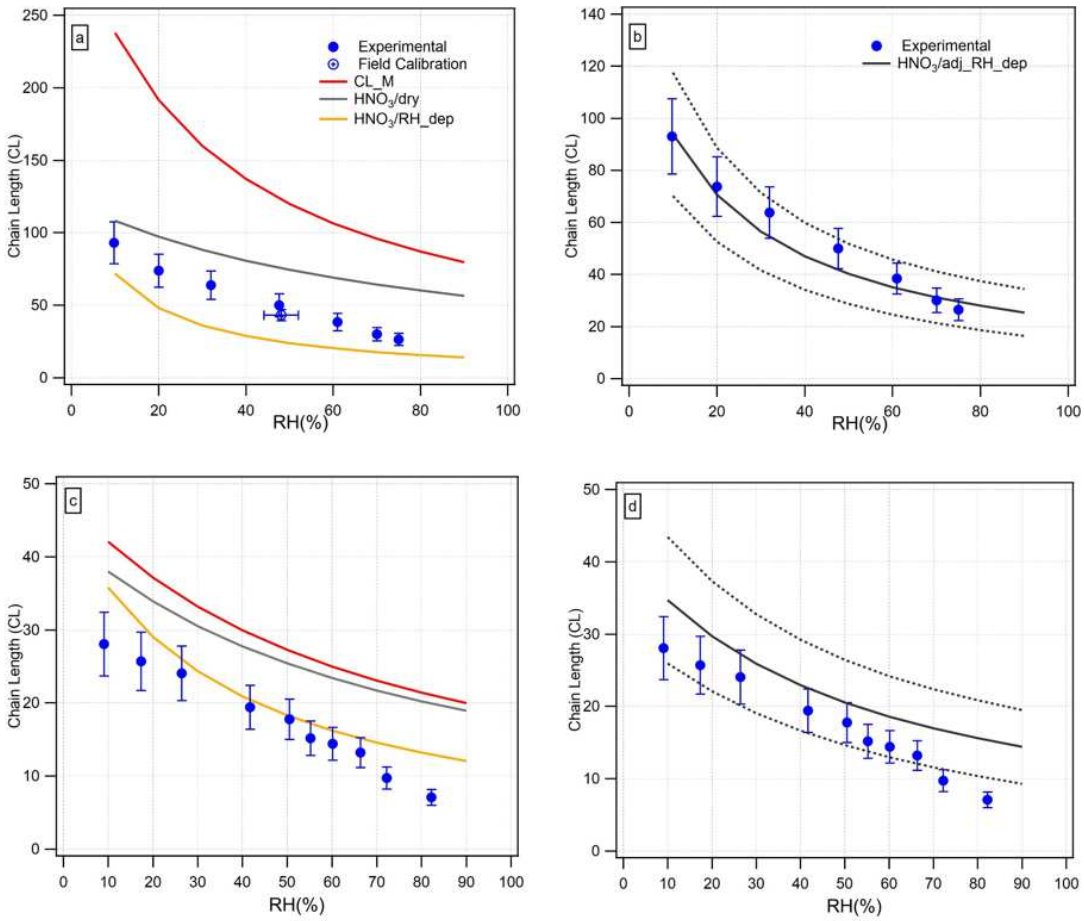

Figure 5. Dependences of experimental (markers) and modeled (lines) CL on RH for the PERCA (panels a and b) and ECHAMP (panels c and d) approaches (T = 23±2°C). The empty circle represents calibration experiments performed in the field (see section Field Testing). Uncertainty on experimental values are 1σ. Panels b,d: dotted lines are uncertainty on modelled values. See section 2.3 for the modeling scenarios.

3.4 Quantification of $T_{(RO2)}$ for several RO_2 radicals

As mentioned in the introduction section, PERCA and ECHAMP techniques rely on the conversion of RO_2 radicals into HO_2 in order to initiate the amplification chemistry. The propagation reactions involved in this process will only transmit a certain fraction of each RO_2, depending on their organic nitrate (R1b) and nitrite (R2-R3) yields. As a consequence, PERCA and ECHAMP techniques will be blind to the fraction of RO_2 radicals that is not propagated to HO_2. It is important to ensure that PERCA or ECHAMP measurements can be compared to model simulations when each modeled peroxy radical concentration is weighted by a transmission factor derived from known organic nitrate and nitrite yields.

Experiments were performed to (i) quantify $T_{(RO2)}$ (Eq. 6-7) for a large suite of peroxy radicals and to (ii) contrast measured $T_{(RO2)}$ values to calculations based on organic nitrate and nitrite yields used in atmospheric models for each RO_2. HO_2 and thirteen organic peroxy radicals were produced from the oxidation of CO and VOCs reported in Table 1 as described in the experimental section. These experiments were performed at 50% RH and ambient temperature (23±2°C) using the ECHAMP approach and operating conditions set to their optimum values as reported in Table 2.

Due to the large concentration of O_2 in ambient air, nitrite formation is negligible (< 3%) for all RO radicals generated in these experiments, with the exception of methoxyl (CH_3O) which exhibits a 5-fold lower rate constant with O_2. Under normal conditions of temperature and pressure (298 K and 1 atm) and using operating conditions reported in Table 2, the nitrite formation yield is estimated to be 8.7% for CH_3O. This higher nitrite yield only concerns the oxidation of acetaldehyde due to the formation of an alkoxyl radical which decomposes to form CH_3O_2.

The measured $T_{(RO2)}$ values are displayed in Table 3 and Figure 6 as a function of an average yield for nitrate formation. The nitrate yields used in these calculations are from MCM V3.2. This figure clearly indicates that there is a relationship between the two variables, with a decrease of $T_{(RO2)}$ when the yield increases, limonene and β-pinene derived peroxy radicals exhibiting the lowest $T_{(RO2)}$ and highest nitrate yields of approximately 77% and 23%, respectively. These results are consistent with observations reported by Ashbourn et al. (1998), showing that R1b becomes more significant for large alkyl peroxy radicals, which in turn leads to $T_{(RO2)}$ values lower than unity. While $T_{(RO2)}$ values are scattered within ±10% around the 1:1 line, it is surprising that 9 of the 12 experiments are lower than the 1:1 line. These lower-than-expected values are likely due to the combination of R1b removal reactions and the injection of large concentrations of VOCs in the calibrator to convert OH into peroxy radicals, which, when introduced in the reactor ran under background mode, can lead to a small amplification of the radicals. Tests performed by introducing different concentrations of isoprene in the calibrator showed that the CL is underestimated by less than 10% for this compound under experimental conditions reported in this study. This would bring $T_{(RO2)}$ for isoprene in very good agreement with the known nitrate yield. A similar impact is expected for the other $T_{(RO2)}$ values measured in this study. In addition, it is interesting to note that lower-than-expected $T_{(RO2)}$ values could also be partly due to NO in homogeneities when ambient air is mixed with the reagents, leading to local concentrations of NO larger than 1 ppm, which in turn can lead to a higher nitrite yield for each RO radical. Indeed, experimental determinations of $T_{(RO2)}$ provide values

517 which are integrated over the reaction time when the reagents are getting mixed with ambient air (NO
518 getting diluted down to 1 ppm). Overall, these results indicate that known nitrate and nitrite yields can be
519 used to scale modelled concentrations of peroxy radicals for comparison with ECHAMP measurements
520 with an uncertainty better than 10%.

521 It is important to note that these scaling factors will be different for the PERCA approach since a higher
522 NO mixing ratio is used to generate the amplification chemistry. The RO_2-to-HO_2 conversion step will be
523 less efficient due to a higher formation rate of organic nitrites. The nitrite yields are expected to increase
524 from 2-3% to 12-18% for most of the RO radicals used in this study, with a higher increase for CH_3O
525 whose nitrite yield will be close to 36%.

526 **Table 3: RO_2 to HO_2 transmission – $T_{(RO2}$**

527

528

529

VOC	*$RONO_2$ yield MCM V3.2 (%)*	$T_{(RO2)}$
Isoprene	10.7	0.84
Limonene	22.8	0.65
m-xylene	7.3	0.91
β-pinene	23.3	0.66
Acetaldehyde	0.1	0.95
Pentane	14.1	0.92
3-methylpentane	12.4	0.74
Cyclohexane	15.0	0.87
Toluene	8.7	0.72
1-pentene	5.9	0.88
Cyclopentene	*4.5**	0.84

* Reference: (Perring et al., 2013)

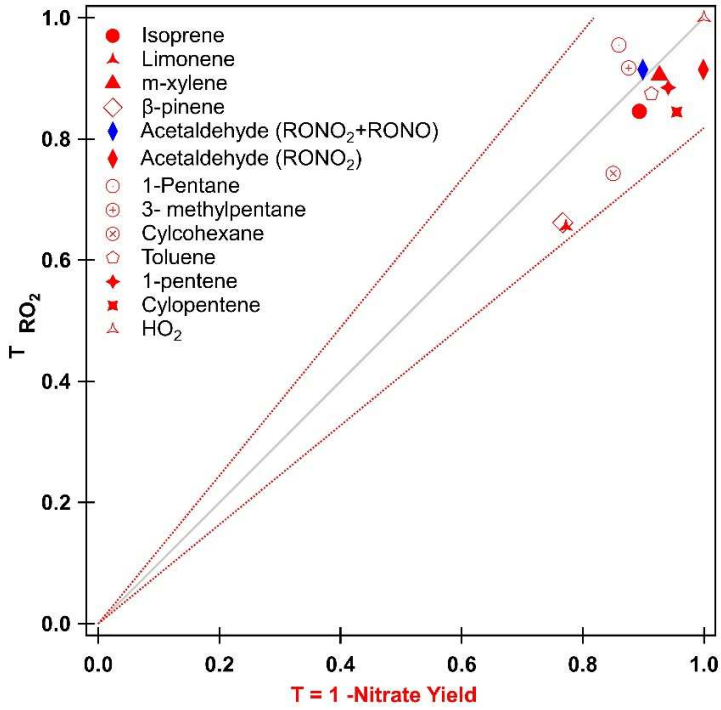

Figure 6: Dependence of $T_{(RO2)}$ (ECHAMP approach) on average organic nitrate yields. The blue symbol for acetaldehyde accounts for nitrate & nitrite formation (see text). Plain grey line is 1:1 and dashed red lines are 1.10:1 and 0.90:1.

3.5 Field deployment of the chemical amplifier

The chemical amplifier was first tested in an urban area, close to our laboratory, in the city of Douai, France. These measurements were performed with the PERCA approach, i.e. using CO and NO as reagents (operating conditions from Table 2). The measurements were conducted over 3 consecutive days in April 2018 using the sequence shown in Figure S2 (supplementary material), which in turn led to a time resolution of 6-min. The overall meteorological conditions allowed to run the instrument under optimal conditions since these 3 days were characterized by clear skies, ambient temperatures between 8 and 25°C, and RH values ranging from 35 to 90%. The only exception was a light rain in the early morning of 21 April, during which RH reached 100%. The peroxy radical measurements are shown in Figure 7 together with the CL calculated at the measured RH values. The latter varied from approximately 10 up to 75. RO_2+HO_2 mixing ratios ranged from the detection limit up to 20 ppt around 2 pm local time (UTC+2), with sustained mixing ratios of 5-10 ppt during the late afternoon and nighttime. The magnitude of the

measured RO_2+HO_2 mixing ratios and their diurnal variations are similar to trends reported in studies performed at measurements sites under urban influences (Tan et al., 2018; Whalley et al., 2018; Wood and Charest, 2014).

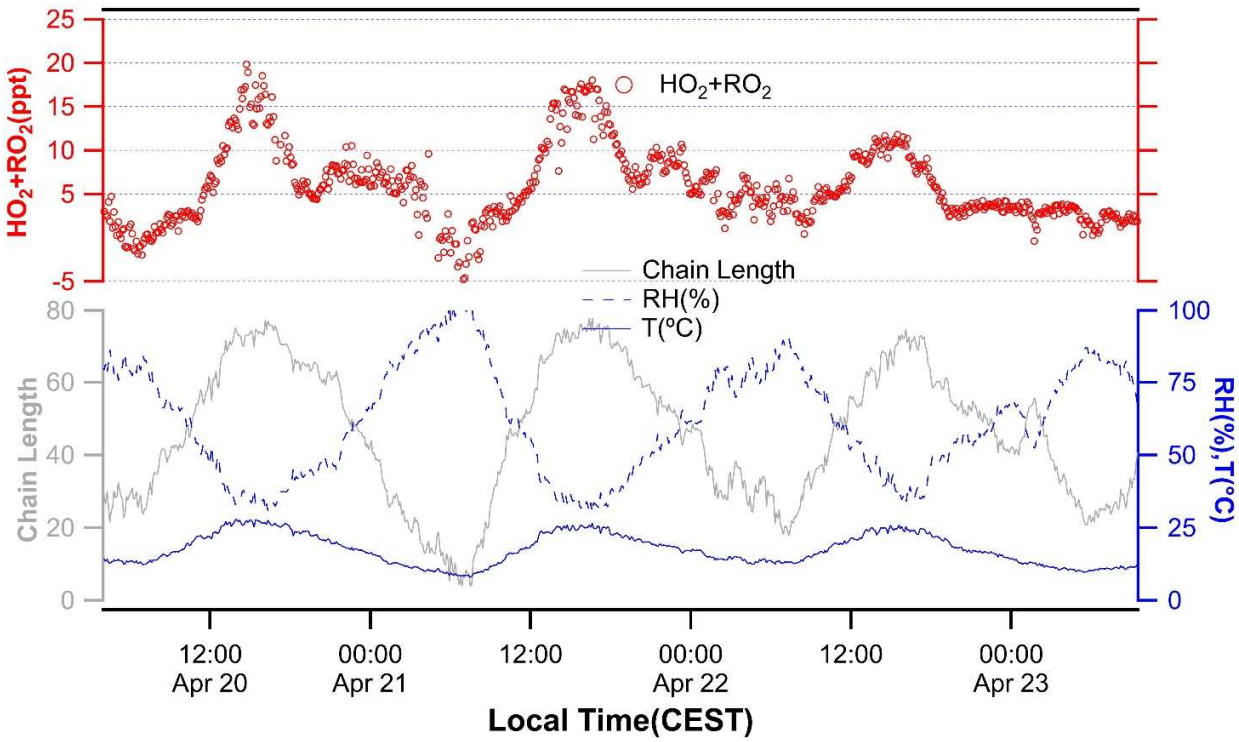

Figure 7: Peroxy radical measurements performed in Douai (France) by chemical amplification using the PERCA approach

This instrument was then deployed in the Landes forest (France) from 2 to 26 July 2018 as part of the CERVOLAND (Characterization of emissions and reactivity of volatile organic compounds in the Landes forest) field campaign. This forest is mainly composed of pine trees (Pinus Pinaster), which are strong emitters of monoterpenes such as α- and β-pinene. The instrument was coupled to a newly designed 9-m^3 Teflon photo-reactor to investigate in-situ the oxidation of biogenic VOCs (BVOCs). Several experiments were conducted by flushing the photo-reactor with ambient air at different times of the day (nighttime, daytime) to trap air masses characterized by different chemical compositions. Oxidation experiments were then performed either in the dark or under solar irradiation. Here, we present peroxy radical measurements from one experiment when the photo-reactor was flushed with ambient air during nighttime for 90

minutes. The air mass trapped in the photo-reactor was loaded with large mixing ratios of monoterpenes (14 ppb) and sesquiterpenes (50 ppt). The ambient ozone mixing ratio was low (12-14 ppb) during the flushing period. The air mass was kept in the dark until 12 pm, BVOCs slowly reacting O_3 away (2-4 ppb around 11 am), and was then exposed to solar radiations until 8 pm by uncovering the photo-reactor. Figure 8 displays the peroxy radical measurements during these two periods.

Peroxy radicals slowly decreased together with O_3 (O3 42E, Environnement SA) from 1 to 9 am. The mixing ratios dropped from 10 to 2 ppt, and 14 to 2 ppb for peroxy radicals and O_3, respectively. O_3-BVOC reactions were likely the main source of radicals during this time period. Peroxy radicals slowly increased from 9 am to 12 am together with the temperature, indicating that thermo-labile precursors of radicals may have been present in the photo-reactor. Once the photo-reactor was uncovered, peroxy radicals rapidly increased from 6 ppt up to 45 ppt around 3 pm. The latter is similar to previously reported peroxy radicals mixing ratios in forested areas (Stone et al., 2012; Vaughan et al., 2012; Wolfe et al., 2014). During this time period peroxy radical measurements are well correlated with $j(NO_2)$ measured above the photo-reactor (fast CCD spectroradiometer from METCON meteorologieconsult gmbh). Interestingly, O_3 increased at a rate of 3-4 ppb h^{-1} from 12 to 3 pm, reaching a plateau at approximately 20 ppb. These results will be presented in detail in a forthcoming publication.

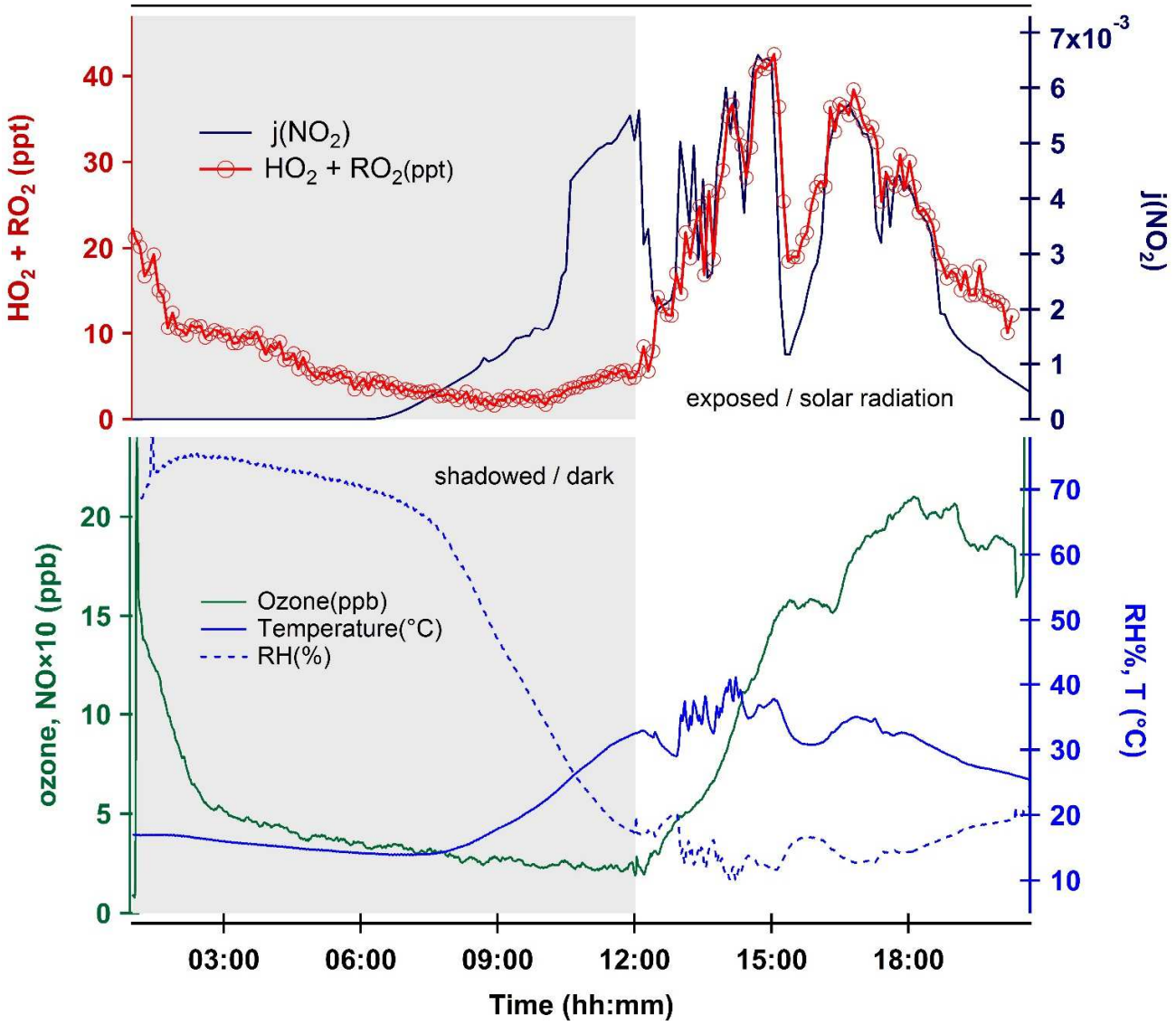

584
585
586 **Figure 8: Peroxy radical measurements performed in a mobile photo-reactor during the CERVOLAND 2018 field**
587 **campaign**
588
589

590 ## 3.6 Estimation of the detection limit

591 Lower bounds for the detection limit can be derived from the measurement noise of the 2 CAPS monitors
592 and the RH-dependent CL, assuming that no other sources of noise are present. Measurements of NO_2 by
593 the two CAPS analyzers used in this work exhibit precisions of 10 and 16 ppt (1σ) when zero air is

sampled, which translate into detection limits (3σ) of 30 and 48 ppt for 70-seconds of integration (70 occurrences of 1-s NO_2 measurements averaged within each measurement step of 90-s, see supplementary material). This leads to detection limits of 1.3, 2.0, and 3.3 ppt for the ECHAMP approach at RH values of 10, 50, and 80%, respectively, for a total measurement time of 6 min (see measurement sequence in the experimental section). For the PERCA approach, the same procedure leads to detection limits of 0.3, 0.6, and 1.4 ppt at 10, 50, and 80% RH, respectively.

However, detection limits for ambient air measurements are expected to be significantly higher due additional sources of noise such as small fluctuations in reagent flow rates, switches of solenoid valves, and changes in ambient concentrations of NO_2 and O_3, which will degrade the precision on ΔNO_2. In order to better estimate limits of detection, both reactors were run in background mode for long time periods of 3-10 hours during the CERVOLAND field campaign. An experiment of this type is shown in the supplementary material (S4), where ΔNO_2/CL is plotted as a function of time for RH values ranging from 20-30%. A statistical analysis of this series indicate that the mean value of 0.03 ± 0.04 ppt is not statistically significant. The standard deviation of 0.3 ppt translates into a detection limit (3σ) of 0.9 ppt. Assuming that ΔNO_2 is not dependent on RH, since peroxy radicals are not amplified, this would translate into detection limits of 0.7, 1.3, and 3.0 ppt at RH values of 10, 50, and 80 %, respectively. These values are approximately 2 times higher than values calculated from the noise of the CAPS monitors. While these values may still underestimate the detection limit in ambient air, since the O_3 and NO_2 variability is reduced in the photo-reactor, it is clear that detection limits on the order of a few ppt are achievable using the PERCA approach. The ECHAMP approach, which has yet to be tested in the field on this instrument, should exhibit detection limits that are approximately 3 times higher.

4 Conclusion

This publication presents the development of a chemical amplifier for ground-based measurements of peroxy radicals in the troposphere. This instrument was used in the laboratory to compare two different approaches regarding the radical amplification chemistry, including the use of CO/NO (PERCA) or ethane/NO (ECHAMP) as reagent gases. Tests performed to identify optimum conditions leading to the highest sensitivity, i.e. the largest chain length, indicate that 10% CO and 6 ppm NO should be used for the PERCA approach, while 2.1% ethane and 0.9 ppm NO are better for ECHAMP. These optimum conditions lead to chain lengths values of approximately 55 and 15 at 50% RH for the PERCA and

623 ECHAMP approaches, respectively. The RH-dependence of the CL was also investigated for both
624 approaches. It was found that the CL decreases with RH, in agreement with previously published studies.
625 The magnitude of the decrease is slightly lower for the ECHAMP technique, with a decrease by a factor 3
626 and 2.7 for the PERCA and ECHAMP approaches, respectively, when RH is increased from 10 to 70% at
627 23±2°C.

628 The amplification chemistry was modelled using MCM v3.2 for comparison to experimental observations.
629 The model/measurement comparison indicates that modeled CL values overestimate experimental
630 observations by a factor of approximately 2. Additional simulations conducted to assess whether the
631 formation of HNO_3 from HO_2+ NO could impact the CL of chemical amplifiers highlighted that using the
632 yield reported under dry conditions, and a 2-fold lower-than-reported water-dependence for this yield,
633 provides a reasonable description of the CL-dependence on reagent gases and RH for both PERCA and
634 ECHAMP. However, the model overestimation of the ECHAMP CL and underestimation of the PERCA
635 CL seems to indicate that our understanding of the amplification chemistry is still incomplete and deserves
636 addition scrutiny.

637 The sensitivity of the chemical amplifier to a large range of RO_2 radicals was quantified to determine
638 whether PERCA and ECHAMP measurements can be compared to model simulations when the
639 concentration of each modelled peroxy radical is weighted by a transmission factor derived from known
640 organic nitrate and nitrite yields. This work showed that transmission factors can be calculated from
641 known kinetic parameters and ambient conditions for the pool of organic peroxy radicals tested in this
642 study.

643 Finally, ambient testing of this chemical amplifier using the PERCA approach showed that this instrument
644 is capable of measuring ambient concentrations of HO_2+RO_2 at levels higher than 1-4 ppt under RH
645 conditions up to 90% once the RH-dependence of the CL has been correctly characterized. Comparisons
646 of the PERCA and ECHAMP techniques to other techniques capable of measuring peroxy radicals would
647 be useful to provide more insight into the accuracy of chemical amplifiers.

648

Acknowledgments

This work was supported by the French national program LEFE/CHAT INSU. This work was also funded by the French National Research Agency (ANR-11-LABX-0005-01) and the European Funds for Regional Economic Development (FEDER) through the CaPPA (Chemical and Physical Properties of the Atmosphere) project. The CERVOLAND field campaign was supported by the French Environment & Energy Management Agency (Ademe) through the PRIMEQUAL program. This work also benefited from funding from the Région Hauts-de-France, the Ministère de l'Enseignement Supérieur et de la Recherche and the European Fund for Regional Economic Development through the CLIMIBIO project.

The authors want to thank Dr. Sasha Kukui for the loan of a radical calibration source, Prof. Eric Villenave, Dr. Emillie Perraudin and Dr. Pierre-Marie Flaud for the organization of the CERVOLAND field campaign, and Prof. Ezra Wood for useful discussions on the ECHAMP and PERCA techniques.

References

Archibald, A.T., Levine, J.G., Abraham, N.L., Cooke, M.C., Edwards, P.M., Heard, D.E., Jenkin, M.E., Karunaharan, A., Pike, R.C., Monks, P.S., Shallcross, D.E., Telford, P.J., Whalley, L.K., Pyle, J.A., 2011. Impacts of HOx regeneration and recycling in the oxidation of isoprene: Consequences for the composition of past, present and future atmospheres. Geophys. Res. Lett. 38, n/a-n/a. https://doi.org/10.1029/2010GL046520

Ashbourn, S.F.M., Jenkin, M.E., Clemitshaw, K.C., 1998. Laboratory Studies of the Response of a Peroxy Radical Chemical Amplifier to HO2 and a Series of Organic Peroxy Radicals. J. Atmospheric Chem. 29, 233–266. https://doi.org/10.1023/a:1005992316512

Atkinson, R., 2003. Kinetics of the gas-phase reactions of OH radicals with alkanes and cycloalkanes. Atmos Chem Phys 3, 2233–2307. https://doi.org/10.5194/acp-3-2233-2003

Atkinson, R., 1986. Kinetics and mechanisms of the gas-phase reactions of the hydroxyl radical with organic compounds under atmospheric conditions. Chem. Rev. 86, 69–201. https://doi.org/10.1021/cr00071a004

Atkinson, R., Aschmann, S.M., Carter, W.P.L., Winer, A.M., Pitts, J.N., 1982. Alkyl nitrate formation from the nitrogen oxide (NOx)-air photooxidations of C2-C8 n-alkanes. J. Phys. Chem. 86, 4563–4569. https://doi.org/10.1021/j100220a022

Atkinson, R., Baulch, D.L., Cox, R.A., Crowley, J.N., Hampson, R.F., Hynes, R.G., Jenkin, M.E., Rossi, M.J., Troe, J., IUPAC Subcommittee, 2006. Evaluated kinetic and photochemical data for atmospheric chemistry: Volume II – gas phase reactions of organic species. Atmos Chem Phys 6, 3625–4055. https://doi.org/10.5194/acp-6-3625-2006

Atkinson, R., Baulch, D.L., Cox, R.A., Jr, R.F.H., Kerr, J.A., Rossi, M.J., Troe, J., 1997. Evaluated Kinetic, Photochemical and Heterogeneous Data for Atmospheric Chemistry: Supplement V. IUPAC Subcommittee on Gas Kinetic Data Evaluation for Atmospheric Chemistry. J. Phys. Chem. Ref. Data 26, 521–1011. https://doi.org/10.1063/1.556011

Berresheim, H., Elste, T., Tremmel, H.G., Allen, A.G., Hansson, H.C., Rosman, K., Dal Maso, M., Mäkelä, J.M., Kulmala, M., O'Dowd, C.D., 2002. Gas-aerosol relationships of H2SO4, MSA, and OH: Observations in the coastal marine boundary layer at Mace Head, Ireland. J. Geophys. Res. Atmospheres 107, PAR 5-1-PAR 5-12. https://doi.org/10.1029/2000JD000229

Braure, T., Bedjanian, Y., Romanias, M.N., Morin, J., Riffault, V., Tomas, A., Coddeville, P., 2014. Experimental Study of the Reactions of Limonene with OH and OD Radicals: Kinetics and Products. J. Phys. Chem. A 118, 9482–9490. https://doi.org/10.1021/jp507180g

Butkovskaya, N., Rayez, M.-T., Rayez, J.-C., Kukui, A., Le Bras, G., 2009. Water Vapor Effect on the HNO3 Yield in the HO2 + NO Reaction: Experimental and Theoretical Evidence. J. Phys. Chem. A 113, 11327–11342. https://doi.org/10.1021/jp811428p

Butkovskaya, N., Kukui, A., Le Bras, G., 2007. HNO3 Forming Channel of the HO2 + NO Reaction as a Function of Pressure and Temperature in the Ranges of 72−600 Torr and 223−323 K. J. Phys. Chem. A 111, 9047–9053. https://doi.org/10.1021/jp074117m

Calvert, J., Mellouki, A., Orlando, J., 2011. Mechanisms of atmospheric oxidation of the oxygenates. OUP USA.

Cantrell, C.A., Stedman, D.H., Wendel, G.J., 1984. Measurement of atmospheric peroxy radicals by chemical amplification. Anal. Chem. 56, 1496–1502. https://doi.org/10.1021/ac00272a065

Cantrell, C.A., Zimmer, A., Tyndall, G.S., 1997. Absorption cross sections for water vapor from 183 to 193 nm. Geophys. Res. Lett. 24, 2195–2198. https://doi.org/10.1029/97GL02100

Clemitshaw, K.C., Carpenter, L.J., Penkett, S.A., Jenkin, M.E., 1997. A calibrated peroxy radical chemical amplifier for ground-based tropospheric measurements. J. Geophys. Res. Atmospheres 102, 25405–25416. https://doi.org/10.1029/97JD01902

Creasey, D.J., Evans, G.E., Heard, D.E., Lee, J.D., 2003. Measurements of OH and HO2 concentrations in the Southern Ocean marine boundary layer. J. Geophys. Res. Atmospheres 108, n/a-n/a. https://doi.org/10.1029/2002JD003206

Creasey, D.J., Heard, D.E., Lee, J.D., 2000. Absorption cross-section measurements of water vapour and oxygen at 185 nm. Implications for the calibration of field instruments to measure OH, HO2 and RO2 radicals. Geophys. Res. Lett. 27, 1651–1654. https://doi.org/10.1029/1999GL011014

Dusanter, S., Vimal, D., Stevens, P.S., 2008. Technical note: Measuring tropospheric OH and HO_2 by laser-induced fluorescence at low pressure. A comparison of calibration techniques. Atmos Chem Phys 8, 321–340. https://doi.org/10.5194/acp-8-321-2008

Dusanter, S., Vimal, D., Stevens, P.S., Volkamer, R., Molina, L.T., Baker, A., Meinardi, S., Blake, D., Sheehy, P., Merten, A., Zhang, R., Zheng, J., Fortner, E.C., Junkermann, W., Dubey, M., Rahn, T., Eichinger, B., Lewandowski, P., Prueger, J., Holder, H., 2009. Measurements of OH and HO_2 concentrations during the MCMA-2006 field campaign – Part 2: Model comparison and radical budget. Atmos Chem Phys 9, 6655–6675. https://doi.org/10.5194/acp-9-6655-2009

Edwards, G.D., Cantrell, C.A., Stephens, S., Hill, B., Goyea, O., Shetter, R.E., Mauldin, R.L., Kosciuch, E., Tanner, D.J., Eisele, F.L., 2003. Chemical Ionization Mass Spectrometer Instrument for the Measurement of Tropospheric HO2 and RO2. Anal. Chem. 75, 5317–5327. https://doi.org/10.1021/ac034402b

Elrod, M.J., 2011. Kinetics Study of the Aromatic Bicyclic Peroxy Radical + NO Reaction: Overall Rate Constant and Nitrate Product Yield Measurements. J. Phys. Chem. A 115, 8125–8130. https://doi.org/10.1021/jp204308f

ESPADA, C., GROSSENBACHER, I., FORD, K., COUCH, T., SHEPSON, P.B., 2005. The production of organic nitrates from various anthropogenic volatile organic compounds. Int. J. Chem. Kinet. 37, 675–685.

Faloona, I.C., Tan, D., Lesher, R.L., Hazen, N.L., Frame, C.L., Simpas, J.B., Harder, H., Martinez, M., Di Carlo, P., Ren, X., 2004. A laser-induced fluorescence instrument for detecting tropospheric OH and HO2: Characteristics and calibration. J. Atmospheric Chem. 47, 139–167.

Finlayson-Pitts, B.J., Pitts, J.N. (Eds.), 2000. Acknowledgments, in: Chemistry of the Upper and Lower Atmosphere. Academic Press, San Diego, pp. xxi–xxii. https://doi.org/10.1016/B978-012257060-5/50002-2

Green, T.J., Reeves, C.E., Fleming, Z.L., Brough, N., Rickard, A.R., Bandy, B.J., Monks, P.S., Penkett, S.A., 2006. An improved dual channel PERCA instrument for atmospheric measurements of peroxy radicals. J. Environ. Monit. 8, 530–536. https://doi.org/10.1039/B514630E

Griffith, S.M., Hansen, R.F., Dusanter, S., Michoud, V., Gilman, J.B., Kuster, W.C., Veres, P.R., Graus, M., de Gouw, J.A., Roberts, J., Young, C., Washenfelder, R., Brown, S.S., Thalman, R., Waxman, E., Volkamer, R., Tsai, C., Stutz, J., Flynn, J.H., Grossberg, N., Lefer, B., Alvarez, S.L., Rappenglueck, B., Mielke, L.H., Osthoff, H.D., Stevens, P.S., 2016. Measurements of hydroxyl and hydroperoxy radicals during CalNex-LA: Model comparisons and radical budgets. J. Geophys. Res. Atmospheres 121, 4211–4232. https://doi.org/10.1002/2015JD024358

Griffith, S.M., Hansen, R.F., Dusanter, S., Stevens, P.S., Alaghmand, M., Bertman, S.B., Carroll, M.A., Erickson, M., Galloway, M., Grossberg, N., Hottle, J., Hou, J., Jobson, B.T., Kammrath, A., Keutsch, F.N., Lefer, B.L., Mielke, L.H., O'Brien, A., Shepson, P.B., Thurlow, M., Wallace, W., Zhang, N., Zhou, X.L., 2013. OH and HO_2 radical chemistry during PROPHET 2008 and CABINEX 2009 – Part 1: Measurements and model comparison. Atmos Chem Phys 13, 5403–5423. https://doi.org/10.5194/acp-13-5403-2013

Hastie, D.R., Weissenmayer, M., Burrows, J.P., Harris, G.W., 1991. Calibrated chemical amplifier for atmospheric ROx measurements. Anal. Chem. 63, 2048–2057. https://doi.org/10.1021/ac00018a029

Heard, D.E., Pilling, M.J., 2003. Measurement of OH and HO2 in the Troposphere. Chem. Rev. 103, 5163–5198. https://doi.org/10.1021/cr020522s

Hendrik Fuchs, Frank Holland, Andreas Hofzumahaus, 2008. Measurement of tropospheric RO2 and HO2 radicals by a laser-induced fluorescence instrument. Rev. Sci. Instrum. 79, 084104. https://doi.org/10.1063/1.2968712

753 Hernández, M.D.A., Burkert, J., Reichert, L., Stöbener, D., Meyer-Arnek, J., Burrows, J.P., Dickerson, R.R.,
754 Doddridge, B.G., 2001. Marine boundary layer peroxy radical chemistry during the AEROSOLS99 campaign:
755 Measurements and analysis. J. Geophys. Res. Atmospheres 106, 20833–20846.
756 https://doi.org/10.1029/2001JD900113
757 Hornbrook, R.S., Crawford, J.H., Edwards, G.D., Goyea, O., Mauldin Iii, R.L., Olson, J.S., Cantrell, C.A., 2011.
758 Measurements of tropospheric HO_2 and RO_2 by oxygen dilution modulation and chemical ionization mass
759 spectrometry. Atmos Meas Tech 4, 735–756. https://doi.org/10.5194/amt-4-735-2011
760 Horstjann, M., Andrés Hernández, M.D., Nenakhov, V., Chrobry, A., Burrows, J.P., 2014. Peroxy radical detection
761 for airborne atmospheric measurements using absorption spectroscopy of NO_2. Atmos Meas Tech 7,
762 1245–1257. https://doi.org/10.5194/amt-7-1245-2014
763 Kartal, D., Andrés-Hernández, M.D., Reichert, L., Schlager, H., Burrows, J.P., 2010. Technical Note: Characterisation
764 of a DUALER instrument for the airborne measurement of peroxy radicals during AMMA 2006. Atmos
765 Chem Phys 10, 3047–3062. https://doi.org/10.5194/acp-10-3047-2010
766 Kroll, J.H., Seinfeld, J.H., 2008. Chemistry of secondary organic aerosol: Formation and evolution of low-volatility
767 organics in the atmosphere. Atmos. Environ. 42, 3593–3624.
768 http://dx.doi.org/10.1016/j.atmosenv.2008.01.003
769 Kukui, A., Ancellet, G., Le Bras, G., 2008. Chemical ionisation mass spectrometer for measurements of OH and
770 Peroxy radical concentrations in moderately polluted atmospheres. J. Atmospheric Chem. 61, 133–154.
771 https://doi.org/10.1007/s10874-009-9130-9
772 Lew, M.M., Dusanter, S., Stevens, P.S., 2018. Measurement of interferences associated with the detection of the
773 hydroperoxy radical in the atmosphere using laser-induced fluorescence. Atmos Meas Tech 11, 95–109.
774 https://doi.org/10.5194/amt-11-95-2018
775 Liu, Y., Morales-Cueto, R., Hargrove, J., Medina, D., Zhang, J., 2009. Measurements of Peroxy Radicals Using
776 Chemical Amplification−Cavity Ringdown Spectroscopy. Environ. Sci. Technol. 43, 7791–7796.
777 https://doi.org/10.1021/es901146t
778 Liu, Y., Zhang, J., 2014. Atmospheric Peroxy Radical Measurements Using Dual-Channel Chemical Amplification
779 Cavity Ringdown Spectroscopy. Anal. Chem. 86, 5391–5398. https://doi.org/10.1021/ac5004689
780 Mao, J., Jacob, D.J., Evans, M.J., Olson, J.R., Ren, X., Brune, W.H., Clair, J.M.S., Crounse, J.D., Spencer, K.M., Beaver,
781 M.R., Wennberg, P.O., Cubison, M.J., Jimenez, J.L., Fried, A., Weibring, P., Walega, J.G., Hall, S.R.,
782 Weinheimer, A.J., Cohen, R.C., Chen, G., Crawford, J.H., McNaughton, C., Clarke, A.D., Jaeglé, L., Fisher,
783 J.A., Yantosca, R.M., Le Sager, P., Carouge, C., 2010. Chemistry of hydrogen oxide radicals (HO_x) in the
784 Arctic troposphere in spring. Atmos Chem Phys 10, 5823–5838. https://doi.org/10.5194/acp-10-5823-
785 2010
786 Mihelcic, D., Holland, F., Hofzumahaus, A., Hoppe, L., Konrad, S., Müsgen, P., Pätz, H.W., Schäfer, H.J., Schmitz, T.,
787 Volz-Thomas, A., Bächmann, K., Schlomski, S., Platt, U., Geyer, A., Alicke, B., Moortgat, G.K., 2003. Peroxy
788 radicals during BERLIOZ at Pabstthum: Measurements, radical budgets and ozone production. J. Geophys.
789 Res. Atmospheres 108, n/a-n/a. https://doi.org/10.1029/2001JD001014
790 Mihelcic, D., Müsgen, P., Ehhalt, D.H., 1985. An improved method of measuring tropospheric NO2 and RO2 by
791 matrix isolation and electron spin resonance. J. Atmospheric Chem. 3, 341–361.
792 https://doi.org/10.1007/bf00122523
793 Mihele, C.M., Hastie, D.R., 2000. Optimized Operation and Calibration Procedures for Radical Amplifier-Type
794 Detectors. J. Atmospheric Ocean. Technol. 17, 788–794. https://doi.org/10.1175/1520-
795 0426(2000)017<0788:OOACPF>2.0.CO;2
796 Mihele, C.M., Hastie, D.R., 1998. The sensitivity of the radical amplifier to ambient water vapour. Geophys. Res.
797 Lett. 25, 1911–1913. https://doi.org/10.1029/98GL01432
798 Mihele, C.M., Mozurkewich, M., Hastie, D.R., 1999. Radical loss in a chain reaction of CO and NO in the presence of
799 water: Implications for the radical amplifier and atmospheric chemistry. Int. J. Chem. Kinet. 31, 145–152.
800 https://doi.org/10.1002/(SICI)1097-4601(1999)31:2<145::AID-KIN7>3.0.CO;2-M

Miyazaki, K., Parker, A.E., Fittschen, C., Monks, P.S., Kajii, Y., 2010. A new technique for the selective measurement of atmospheric peroxy radical concentrations of HO_2 and RO_2 using a denuding method. Atmos Meas Tech 3, 1547–1554. https://doi.org/10.5194/amt-3-1547-2010

Patchen, A.K., Pennino, M.J., Kiep, A.C., Elrod, M.J., 2007. Direct kinetics study of the product-forming channels of the reaction of isoprene-derived hydroxyperoxy radicals with NO. Int. J. Chem. Kinet. 39, 353–361. https://doi.org/10.1002/kin.20248

Perring, A.E., Pusede, S.E., Cohen, R.C., 2013. An Observational Perspective on the Atmospheric Impacts of Alkyl and Multifunctional Nitrates on Ozone and Secondary Organic Aerosol. Chem. Rev. 113, 5848–5870. https://doi.org/10.1021/cr300520x

Read, K.A., Lewis, A.C., Bauguitte, S., Rankin, A.M., Salmon, R.A., Wolff, E.W., Saiz-Lopez, A., Bloss, W.J., Heard, D.E., Lee, J.D., Plane, J.M.C., 2008. DMS and MSA measurements in the Antarctic Boundary Layer: impact of BrO on MSA production. Atmos Chem Phys 8, 2985–2997. https://doi.org/10.5194/acp-8-2985-2008

Reichert, L., Andrés Hernández, M.D., Stöbener, D., Burkert, J., Burrows, J.P., 2003. Investigation of the effect of water complexes in the determination of peroxy radical ambient concentrations: Implications for the atmosphere. J. Geophys. Res. Atmospheres 108, ACH 4-1-ACH 4-16. https://doi.org/10.1029/2002JD002152

Sadanaga, Y., Matsumoto, J., Sakurai, K., Isozaki, R., Kato, S., Nomaguchi, T., Bandow, H., Kajii, Y., 2004. Development of a measurement system of peroxy radicals using a chemical amplification/laser-induced fluorescence technique. Rev. Sci. Instrum. 75, 864–872. https://doi.org/doi:http://dx.doi.org/10.1063/1.1666985

Sanchez, J., Tanner, D.J., Chen, D., Huey, L.G., Ng, N.L., 2016. A new technique for the direct detection of HO2 radicals using bromide chemical ionization mass spectrometry (Br-CIMS): initial characterization. Atmos Meas Tech 9, 3851–3861. https://doi.org/10.5194/amt-9-3851-2016

Sneep, M., Ubachs, W., 2005. Direct measurement of the Rayleigh scattering cross section in various gases. J. Quant. Spectrosc. Radiat. Transf. 92, 293–310. https://doi.org/10.1016/j.jqsrt.2004.07.025

Sutton, J.A., Driscoll, J.F., 2004. Rayleigh scattering cross sections of combustion species at 266, 355, and 532 nm for thermometry applications. Opt Lett 29, 2620–2622. https://doi.org/10.1364/OL.29.002620

Stevens, P.S., Mather, J.H., Brune, W.H., 1994. Measurement of tropospheric OH and HO2 by laser-induced fluorescence at low pressure. J. Geophys. Res. Atmospheres 99, 3543–3557. https://doi.org/10.1029/93JD03342

Stone, D., Whalley, L.K., Heard, D.E., 2012. Tropospheric OH and HO2 radicals: field measurements and model comparisons. Chem. Soc. Rev. 41, 6348–6404. https://doi.org/10.1039/C2CS35140D

Tan, Z., Lu, K., Hofzumahaus, A., Fuchs, H., Bohn, B., Holland, F., Liu, Y., Rohrer, F., Shao, M., Sun, K., Wu, Y., Zeng, L., Zhang, Y., Zou, Q., Kiendler-Scharr, A., Wahner, A., Zhang, Y., 2018. Experimental budgets of OH, HO$_\mathbf2$ and RO$_\mathbf2$ radicals and implications for ozone formation in the Pearl River Delta in China 2014. Atmospheric Chem. Phys. Discuss. 2018, 1–28. https://doi.org/10.5194/acp-2018-801

Teruel, M.A., Lane, S.I., Mellouki, A., Solignac, G., Le Bras, G., 2006. OH reaction rate constants and UV absorption cross-sections of unsaturated esters. Atmos. Environ. 40, 3764–3772. https://doi.org/10.1016/j.atmosenv.2006.03.003

Vaughan, S., Ingham, T., Whalley, L.K., Stone, D., Evans, M.J., Read, K.A., Lee, J.D., Moller, S.J., Carpenter, L.J., Lewis, A.C., Fleming, Z.L., Heard, D.E., 2012. Seasonal observations of OH and HO_2 in the remote tropical marine boundary layer. Atmospheric Chem. Phys. 12, 2149–2172. https://doi.org/10.5194/acp-12-2149-2012

Volkamer, R., Sheehy, P., Molina, L.T., Molina, M.J., 2010. Oxidative capacity of the Mexico City atmosphere – Part 1: A radical source perspective. Atmos Chem Phys 10, 6969–6991. https://doi.org/10.5194/acp-10-6969-2010

Whalley, L.K., Stone, D., Dunmore, R., Hamilton, J., Hopkins, J.R., Lee, J.D., Lewis, A.C., Williams, P., Kleffmann, J., Laufs, S., Woodward-Massey, R., Heard, D.E., 2018. Understanding in situ ozone production in the

summertime through radical observations and modelling studies during the Clean air for London project (ClearfLo). Atmospheric Chem. Phys. 18, 2547–2571. https://doi.org/10.5194/acp-18-2547-2018

Wolfe, G.M., Cantrell, C., Kim, S., Mauldin III, R.L., Karl, T., Harley, P., Turnipseed, A., Zheng, W., Flocke, F., Apel, E.C., Hornbrook, R.S., Hall, S.R., Ullmann, K., Henry, S.B., DiGangi, J.P., Boyle, E.S., Kaser, L., Schnitzhofer, R., Hansel, A., Graus, M., Nakashima, Y., Kajii, Y., Guenther, A., Keutsch, F.N., 2014. Missing peroxy radical sources within a summertime ponderosa pine forest. Atmos Chem Phys 14, 4715–4732. https://doi.org/10.5194/acp-14-4715-2014

Wolfe, G.M., Thornton, J.A., McKay, M., Goldstein, A.H., 2011. Forest-atmosphere exchange of ozone: sensitivity to very reactive biogenic VOC emissions and implications for in-canopy photochemistry. Atmos Chem Phys 11, 7875–7891. https://doi.org/10.5194/acp-11-7875-2011

Wolfe, G.M., Marvin, M.R., Roberts, S.J., Travis, K.R., Liao, J., 2016. The Framework for 0-D Atmospheric Modeling (F0AM) v3.1. Geosci Model Dev 9, 3309–3319. https://doi.org/10.5194/gmd-9-3309-2016

Wood, E.C., Charest, J.R., 2014. Chemical Amplification - Cavity Attenuated Phase Shift Spectroscopy Measurements of Atmospheric Peroxy Radicals. Anal. Chem. 86, 10266–10273. https://doi.org/10.1021/ac502451m

Wood, E.C., Deming, B.L., Kundu, S., 2017. Ethane-Based Chemical Amplification Measurement Technique for Atmospheric Peroxy Radicals. Environ. Sci. Technol. Lett. 4, 15–19. https://doi.org/10.1021/acs.estlett.6b00438